Optics Letters

High-repetition-rate GaAs-on-SiN mode-locked laser using a Fabry–Pérot cavity

Dongbo Wang,[1,*] Tom Reep,[1] Thi Ngoc Lam Tran,[1,2] Stijn Poelman,[1] Jose Carreira,[3] Camiel Op de Beeck,[3] Stijn Cuyvers,[3] Michael Geiselmann,[3] Jing Zhang,[1] Gunther Roelkens,[1] and Bart Kuyken[1]

[1]Photonics Research Group, INTEC, Ghent University - imec, Technologiepark-Zwijnaarde 126, 9052 Ghent, Belgium
[2]Current address: Chalmers University of Technology, Gothenburg, Sweden
[3]Ligentec SA, Chemin de la Dent d'Oche 1B, EPFL Innovation Park, Bâtiment L, 1024 Écublens, Switzerland
*Dongbo.Wang@UGent.be

Received 15 May 2026; revised 24 June 2026; accepted 7 July 2026; posted 9 July 2026; published 21 July 2026

We demonstrate a 23.3 GHz GaAs-on-SiN mode-locked laser heterogeneously integrated on a commercial SiN platform using micro-transfer printing. A compact Fabry–Pérot cavity with a central saturable absorber enables colliding-pulse, second-harmonic mode locking. The device delivers up to 1 mW on-chip optical power from a single output port and generates eight comb lines within a 10 dB optical bandwidth. The pulse-forming operation is confirmed by autocorrelation measurements, yielding a deconvolved pulse width of 4.8 ps. This approach provides a scalable route toward electrically pumped high-repetition-rate pulse sources for nonlinear SiN photonic circuits.

https://doi.org/10.1364/OL.605625

Introduction. The rapid growth of artificial intelligence (AI) and high-performance computing (HPC) is placing stringent bandwidth and energy-efficiency requirements on optical input/output technologies. Wavelength-division multiplexing is a key strategy for scaling optical link capacity, requiring compact, efficient, and mutually stable multi-wavelength light sources anchored to a fixed frequency grid [1]. Optical frequency combs, consisting of mutually coherent and equally spaced spectral lines, are well suited to this role and can be generated on chip through electro-optic modulation, Kerr and quadratic nonlinearities in microresonators, or semiconductor mode-locked lasers (MLLs) [2–4]. Among these approaches, MLLs are particularly attractive because they generate combs directly via electrical pumping, without the need for an external optical pump. While monolithic quantum-dot MLLs have recently demonstrated 100 GHz O-band operation for datacom transmission with an aggregate throughput of 3.3 Tb/s [5], silicon nitride (SiN) photonics provides a low-loss, broadband, and dispersion-engineered passive platform [6]. Combining III–V gain with SiN circuits has therefore become an important route toward fully integrated, electrically pumped comb lasers for applications beyond datacom, including spectroscopy, ranging, and nonlinear photonics [7,8].

A key advantage of SiN-based MLLs is that the low-loss passive waveguide can be used to form long external cavities, thereby improving the phase-noise performance. This has led to several sub-gigahertz to few-gigahertz demonstrations using micro-transfer printing (μTP) [9,10]. While this long-cavity approach is well-suited for narrow comb spacing and low-noise operation, several emerging nonlinear SiN systems require pulse trains with repetition rates in the tens-of-gigahertz range. In particular, pulse-driven Kerr microresonators can improve the conversion efficiency of low-FSR soliton microcombs, provided that the pump pulse train is matched to the resonator FSR [11,12]. Recent work on a 15 GHz SiN racetrack resonator has shown octave-spanning soliton microcomb generation using picosecond pulse pumping, highlighting the need for integrated high-repetition-rate mode-locked pump sources [13]. High-pulse-energy integrated mode-locked lasers on low-loss SiN have recently been used to directly drive octave-spanning supercontinuum generation, further highlighting the need for SiN-compatible pulsed sources [14]. Reaching this repetition-rate regime in a heterogeneously integrated laser can be achieved by shortening the cavity length or employing harmonic mode locking, while still maintaining stable pulse formation. High-repetition-rate InAs/GaAs quantum-dot comb lasers on silicon have shown second-harmonic comb operation at 31.5 GHz; however, the reported beatnote locking was incomplete, and no clear pulse generation was observed [15]. Therefore, GaAs-on-SiN mode-locked lasers that can generate pulses at tens-of-gigahertz repetition rates are highly desirable for integrated photonics.

In this work, we demonstrate a high-repetition-rate GaAs-on-SiN MLL heterogeneously integrated on a commercial SiN platform using micro-transfer printing. The laser employs a compact Fabry–Pérot (FP) cavity with a central saturable absorber (SA) and two symmetric gain sections, supporting colliding-pulse, second-harmonic mode locking at 23.3 GHz. The device delivers up to 1 mW on-chip optical power from a single output port, with eight regularly spaced comb lines within a 10 dB optical bandwidth and a pulse width of 4.8 ps. These results establish a compact electrically pumped GaAs-on-SiN pulse source compatible with nonlinear SiN photonic systems.

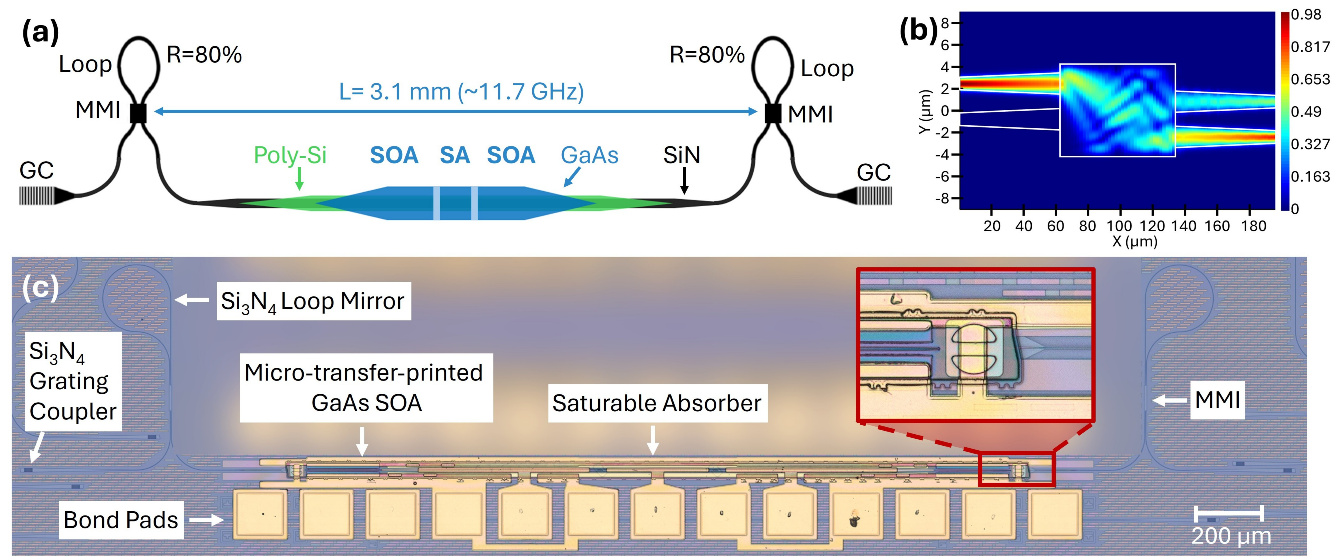

Fig. 1. (a) Schematic of the GaAs-on-SiN Fabry–Pérot (FP) mode-locked laser. (b) Simulated optical field profile of the 72/28 MMI. (c) Optical microscope image of the fabricated device. The inset shows a zoomed-in view of the printed GaAs coupon, which is well aligned with the underlying waveguide.

Device design and fabrication. The device is designed as a GaAs-on-SiN Fabry–Pérot mode-locked laser, as shown in Fig. 1(a). The laser cavity is integrated in the SiN circuit using the layer stack reported in Ref. [16], and is defined by two Sagnac loop mirrors with a designed reflectivity of 80%. In contrast to the directional-coupler-based loop mirrors used in previous work [17], a 72/28 multimode interferometer (MMI) coupler is used here to improve fabrication tolerance and broaden the operating bandwidth. The optical field profile of the MMI, simulated using the EigenMode Expansion solver in Ansys Lumerical MODE, is shown in Fig. 1(b). The unbalanced splitting ratio is obtained by laterally offsetting the access waveguides from the MMI centerline. Grating couplers are used to couple light out of the integrated chip for characterization.

The total cavity length is 3.1 mm, corresponding to a fundamental cavity mode spacing of about 11.7 GHz. The GaAs coupon is 2.18 mm long and contains a 310-μm-long SA located at the cavity midpoint, leaving two symmetric SOA sections on either side. The passive SiN cavity is designed symmetrically to support colliding-pulse, second-harmonic mode locking, for which the pulse repetition rate is twice the fundamental FP mode spacing. To facilitate optical coupling between the SiN waveguide and the GaAs gain section, a polycrystalline silicon (poly-Si) intermediate layer is incorporated to bridge the refractive-index mismatch, enabling efficient evanescent coupling. In the SiN/poly-Si/GaAs optical transition, the poly-Si taper has a 180 nm wide tip to reduce back reflection. Simulations show a coupling efficiency above 96% for lateral misalignments of the printed GaAs coupon up to 1 μm.

An optical microscope image of the fabricated laser is shown in Fig. 1(c). The laser external cavity was fabricated in the 800-nm-thick SiN layer. Before micro-transfer printing, a thin BCB adhesive layer was spin-coated on the SiN target chip to promote bonding of the GaAs coupon. Transfer printing was carried out at room temperature using an X-Celeprint μTP-100 tool. After printing, the BCB was fully cured at 280 °C. The metal redistribution traces and contact pads were then formed by depositing 40 nm Ti and 1 μm Au. Finally, a BCB passivation layer was applied, with openings defined only above the contact pads. This passivation reduces direct exposure of the GaAs tapers and exposed SA section to ambient moisture and oxygen, thereby mitigating potential degradation.

Device characterization. The fabricated device was characterized on a temperature-controlled chuck maintained at 18 °C. Electrical injection and SA bias were applied through a custom RF probe using two Keithley 2400 source measurement units. The optical output was collected from a SiN grating coupler with a cleaved SMF-28 fiber. Owing to the symmetric cavity design, the laser emits from both sides. The optical power reported here was measured from a single output port using an HP 8153A optical power meter and therefore corresponds to half of the total generated power.

Figure 2 shows the light–current–voltage (LIV) characteristics under different SA bias conditions. The current–voltage curve gives a differential resistance of about 3 Ω at 140 mA. Lasing starts at a gain current of 57 mA. Increasing the reverse bias on the SA introduces additional unsaturated SA loss, which shifts the threshold to higher current, while the output power is moderately reduced over the bias range used for mode locking. The on-chip optical power was calibrated using a nearby reference waveguide with identical grating couplers at both ends. The fiber-to-fiber transmission of this reference waveguide was measured before laser characterization and used to convert the fiber-collected power to on-chip power. In the FP lasing regime, the laser delivers up to 1 mW on-chip optical power from a single output port at a gain current of 110 mA. The device enters the mode-locking regime at SA reverse biases above 2 V. The resulting optical and RF characteristics are analyzed in the following discussion.

Figures 3(a) and 3(b) show the optical spectra of the laser at a gain current of 120 mA for SA biases of 0 V and −2.1 V, respectively. At zero SA bias, the device operates as a multimode FP laser. The longitudinal FP modes, with a fundamental spacing of 11.7 GHz, are clearly resolved, but the lack of an RF beatnote indicates that the modes are not phase-locked. Under a −2.1 V SA reverse bias, the optical spectrum transitions

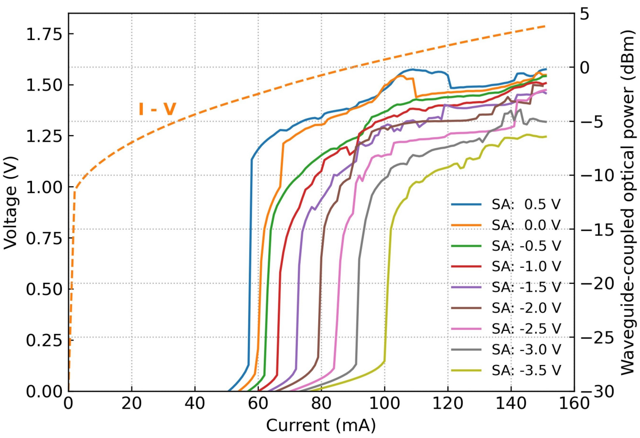

Fig. 2. Light–current–voltage (LIV) characteristics under different SA bias conditions.

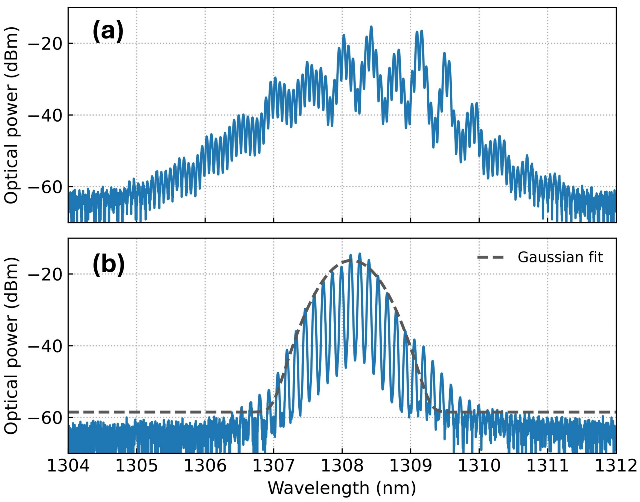

Fig. 3. Optical spectra of the GaAs-on-SiN laser. (a) Multimode FP lasing at 0 V SA bias and (b) mode locking at −2.1 V SA bias. The dashed curve shows a Gaussian fit to the comb-line peak envelope.

into a stable frequency comb centered at 1308 nm, featuring 8 lines across within a 10 dB optical bandwidth. The observed spacing is twice the fundamental FP FSR, consistent with second-harmonic mode locking induced by the colliding-pulse geometry. This is further confirmed by the RF spectrum, which shows a stable beatnote. Further broadening of the optical spectrum could be pursued by engineering the active-region optical confinement and optimizing the gain–absorber design [10].

The RF characterization was performed by coupling the light to a high-speed photoreceiver equipped with a transimpedance amplifier, followed by a Keysight N9010A electrical spectrum analyzer. Figure 4(a) shows a clear RF beatnote at 23.3 GHz, measured over a 0–44 GHz span with a resolution bandwidth (RBW) of 200 kHz. The nearly flat background is mainly attributed to the photoreceiver and analyzer noise floor. This frequency is twice the FP mode spacing, confirming second-harmonic mode locking in agreement with the optical spectrum. Figure 4(b) shows a zoomed-in view of the RF beatnote under passive and hybrid mode-locking conditions. For the hybrid configuration, 30 μW of RF power was injected into the SA section

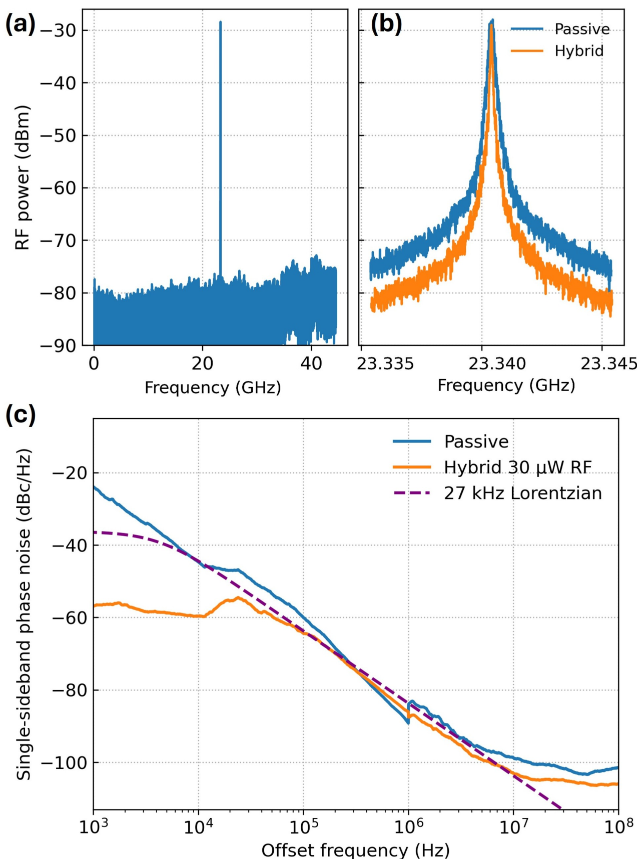

Fig. 4. (a) RF spectrum confirming mode-locked operation. (b) Zoomed-in view of the RF beatnote for passive and hybrid mode locking, measured with a 50 kHz RBW. (c) Single-sideband phase noise (SSB-PN) for passive and hybrid mode locking.

at the repetition frequency. This injection significantly narrows the beatnote and suppresses the noise pedestal compared to the passive state.

The stability of the frequency comb was further evaluated through single-sideband phase-noise (SSB-PN) measurements [18], shown in Fig. 4(c). In the passive regime, the measured SSB-PN trace is well fitted by a Lorentzian linewidth of 27 kHz over the offset-frequency range from 5 kHz to 5 MHz. Hybrid mode locking notably suppresses phase noise below 100 kHz, while the high-offset-frequency noise remains unaffected. This reduction indicates that RF injection primarily mitigates low-frequency technical noise.

Time-domain characterization was performed to confirm stable pulse generation in the mode-locking regime. As shown in Fig. 5(a), the output was detected by a 40 GHz photoreceiver, with the resulting waveform recorded on a high-speed oscilloscope. A stable pulse train is observed with a period of 43 ps, in agreement with the 23.3 GHz repetition rate measured in the RF spectrum. The corresponding single-port pulse energy is calculated to be about 27 fJ, based on an on-chip average power of approximately −2 dBm at this mode-locking condition.

Because the oscilloscope measurement is bandwidth-limited, the individual pulse duration was then characterized using a non-collinear second-harmonic-generation intensity autocorrelator. The laser output was pre-amplified by a praseodymium-doped fiber amplifier (PDFA) to meet the autocorrelator input-power requirement. Figure 5(b) shows the measured intensity

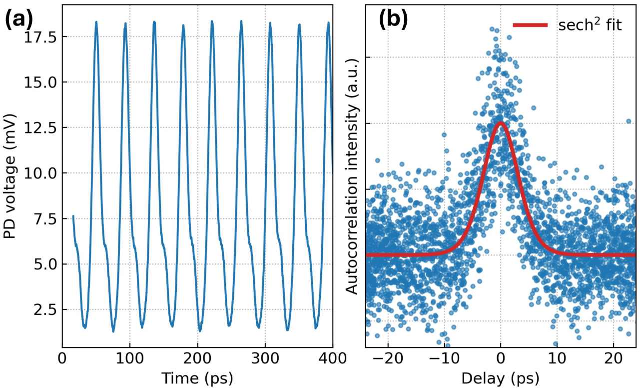

Fig. 5. (a) Pulse train recorded from a 40 GHz photoreceiver. (b) Intensity autocorrelation trace of the pulse.

autocorrelation trace; assuming a sech^2 pulse shape, the deconvolved pulse width is estimated to be 4.8 ps, confirming stable optical pulse generation. Combined with the 0.61 nm optical spectral FWHM obtained from the Gaussian fit, this gives a time-bandwidth product of about 0.51, which is about 1.6 times the transform-limited value for a sech^2 pulse. Uncompensated dispersion in the PDFA and fiber path could further broaden the measured autocorrelation trace, so the extracted pulse width should be regarded as a conservative estimate.

Conclusion and outlook. In conclusion, we have demonstrated a 23.3 GHz GaAs-on-SiN mode-locked laser heterogeneously integrated on a commercial SiN platform via micro-transfer printing. By employing a compact Fabry–Pérot cavity with a centrally located saturable absorber and two symmetrically arranged gain sections, we achieved stable second-harmonic colliding-pulse mode locking. The device delivers up to 1 mW of on-chip optical power from a single output and generates a frequency comb with eight lines across the 10 dB optical bandwidth. Pulse-forming operation is confirmed by a high-extinction RF beatnote, a regular pulse train, and a deconvolved autocorrelation pulse width of 4.8 ps. A remaining practical consideration for the present GaAs-on-SiN lasers is transfer-printing reproducibility, which can influence device-to-device consistency. Moving toward a wafer-scale transfer printing process would provide a route to improved process control and systematic yield optimization.

This electrically pumped pulse source is inherently compatible with nonlinear SiN photonic circuits on the same platform. Its tens-of-gigahertz repetition rate matches the electronically detectable FSRs of SiN microresonators, allowing synchronized pulse pumping for enhanced Kerr-comb and resonant-supercontinuum generation [12,13]. The co-integration of GaAs-on-SiN mode-locked lasers with dispersion-engineered SiN resonators will provide a scalable route toward fully integrated, octave-spanning comb sources for applications in spectroscopy, coherent communications, and optical atomic clocks [19].

Funding. European Innovation Council (101047289, 101158577); European Union (825453, 101070560).

Disclosures. The authors declare no conflicts of interest.

Data availability. Data underlying the results presented in this work are not publicly available at this time but may be obtained from the authors upon reasonable request.

REFERENCES

1. M. Wade, E. Anderson, S. Ardalan, *et al.*, IEEE Micro. **40**, 63 (2020).
2. M. Zhang, B. Buscaino, C. Wang, *et al.*, Nature **568**, 373 (2019).
3. T. J. Kippenberg, A. L. Gaeta, M. Lipson, *et al.*, Science **361**, eaan8083 (2018).
4. L. Chang, S. Liu, and J. E. Bowers, Nat. Photonics **16**, 95 (2022).
5. S. Pan, V. Cao, Y. Feng, *et al.*, Laser Photonics Rev. **20**, e01559 (2026).
6. C. Xiang, W. Jin, and J. E. Bowers, Photon. Res. **10**, A82 (2022).
7. N. Picqué and T. W. Hänsch, Nat. Photonics **13**, 146 (2019).
8. I. Coddington, W. C. Swann, L. Nenadovic, *et al.*, Nat. Photonics **3**, 351 (2009).
9. S. Cuyvers, B. Haq, C. Op de Beeck, *et al.*, Laser Photonics Rev. **15**, 2000485 (2021).
10. M. Billet, S. Cuyvers, S. Poelman, *et al.*, Photonics Res. **12**, A21 (2024).
11. E. Obrzud, S. Lecomte, and T. Herr, Nat. Photonics **11**, 600 (2017).
12. M. H. Anderson, R. Bouchand, J. Liu, *et al.*, Optica **8**, 771 (2021).
13. A. Davydova, M. H. Anderson, Z. Qiu, *et al.*, in *Conference on Lasers and Electro-Optics (CLEO)* (2025), paper SS101_2.
14. Z. Qiu, X. Yang, X. Li, *et al.*, Nature **654**, 57 (2026).
15. T. Renaud, H. Huang, G. Kurczveil, *et al.*, Appl. Phys. Lett. **123**, 011105 (2023).
16. D. Wang, T. Reep, L. T. N. Tran, *et al.*, in *Conference on Lasers and Electro-Optics (CLEO)* (2025), paper PD102_2.
17. A. Hermans, K. Van Gasse, J. Ø. Kjellman, *et al.*, APL Photonics **6**, 096102 (2021).
18. D. Auth, S. Liu, J. Norman, *et al.*, Opt. Express **27**, 27256 (2019).
19. K. Wu, N. P. O'Malley, S. Fatema, *et al.*, Nat. Photonics **19**, 400 (2025).